RSC Advances

This is an *Accepted Manuscript*, which has been through the Royal Society of Chemistry peer review process and has been accepted for publication.

Accepted Manuscripts are published online shortly after acceptance, before technical editing, formatting and proof reading. Using this free service, authors can make their results available to the community, in citable form, before we publish the edited article. This *Accepted Manuscript* will be replaced by the edited, formatted and paginated article as soon as this is available.

You can find more information about *Accepted Manuscripts* in the Information for Authors.

Please note that technical editing may introduce minor changes to the text and/or graphics, which may alter content. The journal's standard Terms & Conditions and the Ethical guidelines still apply. In no event shall the Royal Society of Chemistry be held responsible for any errors or omissions in this *Accepted Manuscript* or any consequences arising from the use of any information it contains.

ROYAL SOCIETY OF CHEMISTRY

www.rsc.org/advances

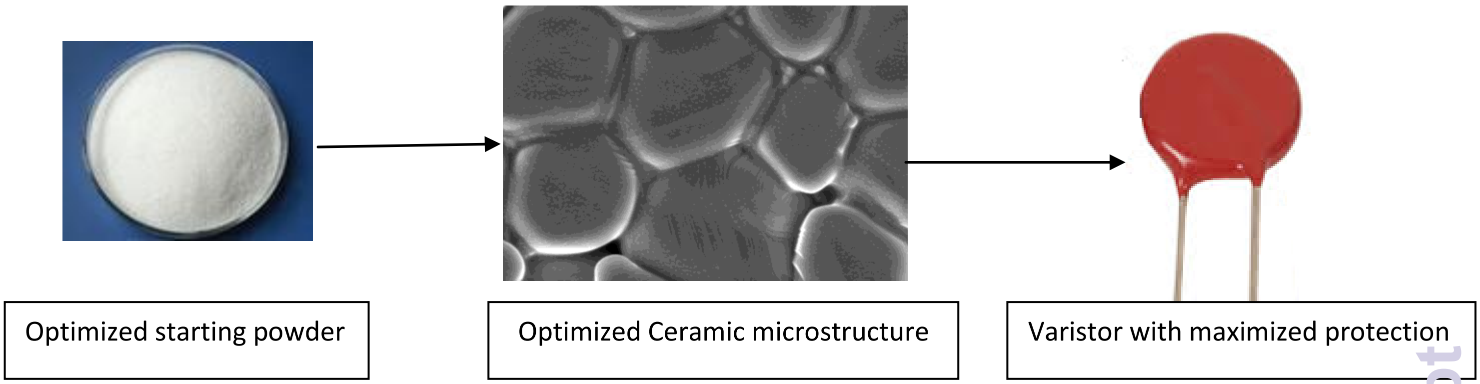

RSC Advances Accepted Manuscript

Cite this: DOI: 10.1039/c0xx00000x
www.rsc.org/xxxxxx

ARTICLE TYPE

Enhance protection of electronic appliances through multivariate modelling and optimization of ceramic core materials in varistor devices

Masoumeh Dorraj[a], Yadollah Abdollahi[a,b*], Suhana Binti Mohd Said[a], Mohd Faizul Bin Mohd Sabri[c], Nor Asrina Sairi[d], Woi Pei Meng[d], Ebrahim Abouzari-lotf[e]

Full Name,*[a] Full Name[a,b] and Full Name[b]

Received (in XXX, XXX) Xth XXXXXXXXX 20XX, Accepted Xth XXXXXXXXX 20XX
DOI: 10.1039/b000000x

E-waste comprises discarded low quality protected electronic appliances which annually accumulates million tons hazardous materials through environment. The protection is provided to control the unwanted voltages that usually generate in the associated electrical circuits by the multi-junction ceramic in the voltage dependent varistor. The ceramic's microstructure consists of ZnO grains that are surrounded by the narrow boundaries of melted specific additives such as Bi_2O_3, TiO_2 and Sb_2O_3. In fact, the boundaries manage the quality of the protection through the certain volume of intrinsic oxygen vacancies transformation which depends on the amounts of the additives. Since the amounts are the ceramic fabrication's initial input variables, the optimization process is capable to improve the quality of the protection (non-linear coefficient) as output of the varistor devices. In this work, the fabrication was designed and then experimentally performed to calculate the non-linear coefficients of the produced varistors as actual responses. The responses were used to obtain the appropriate model for the fabrication by different semi-empirical methods. Afterward, the models predicted the optimized amounts of the additives which maximized the quality of the varistors. The predicted condition was fabricated as final varistors which electrically characterized to compare their nonlinear coefficients as the quality indicator. The comparison has demonstrated that the optimized amounts of Bi_2O_3 (0.5), TiO_2 (0.47) and Sb_2O_3 (0.21) in mol % have provided the very high protective varistor with nonlinear coefficients 28.1. In conclusion, the optimization which has industrial scales up potential warranties the electronic protection that controls the global e-waste.

Introduction

Globally e-waste accumulates millions ton hazardous materials such as heavy metals including lead, mercury, cadmium, halogenated substances into water, soil and air [1]. E-waste comprises discarded electronic appliances, of which anything with a plug even old refrigerators and motorized toothbrushes are disproportionately abundant because of their short lifespan [2]. The electronics are often damaged of repeated exposure to large overvoltages which are generated by electrostatic discharge and electrical overstress such as lightning strikes, power outages tripped circuits, power transitions, power malfunctions, electromagnetic pulses and inductive spikes in the associated circuit [3-4]. Whereas, the electronics are protected by voltage limiting devices such as voltage dependent low voltage varistors and back-to-back zener diodes that are placed at parallel position of the electronics in the associated electrical circuit [5]. The problem is that the diodes are degraded by repeating exposure in large overvoltages due to their low capacity and single p-n junction [6]. On the other hand, the varistors tend to be more stable in AC and DC field over wide range of voltage, a few volts to tens kilovolts and current from micro-amperes to kilo-amperes. However, the varistors have not enough developed and present several drawbacks such as low non-linear properties, high leakage-current, high breakdown-voltage and high degradation for repeating exposure which come from the microstructure of

RSC Advances Accepted Manuscript

ceramic core used in the varistor [7-8]. In the most common varistor, the microstructure consists of highly conductive n-type ZnO grains that are surrounded by the narrow boundaries of melted specific additives [9-10]. The microstructure is fabricated by mixing the appropriate amount of ZnO and the additives (starting powder). Then the mixed powder pressed and sintered at the temperature under the melting point of ZnO [11-12]. Accordingly, the melted additives occupy the ZnO grains boundaries as intergranular layers which navigate the non-linear property by using intrinsic oxygen vacancies transformation [5, 13-21]. Therefore, the origin of the varistor action is attributed to composition of the intergranular layer that is depends on many operation such as type, amount and mixing method of the additives in the starting powders as well as the sintering process [19-21]. The optimum sintering temperatures and holding time for Bi_2O_3 doped ZnO based low voltage varistor were reported from 1200 to 1280 and 1 hour respectively [22]. The stable performance throughout the intergranular layers requires homogenous in terms of its components which is provided by chemical mixing methods (solution coating) of the starting powders [23-24]. The non-linearity as quality of the protection meanly depends on chemical compositions of the materials in intergranular layer which is come from the starting powders [25-26]. For instance, Bi_2O_3 is used as former which is crucial parameter for varistor manufacturing, TiO_2 prevents the vaporization of Bi_2O_3 to facilitate ZnO grain growth, and Sb_2O_3 stabilizes the electrical properties and diminishes the leakage current of the varistor during performance [16, 27-31]. Among the operators, follow up the compositions is very difficult because the layer formulation consists of several high pressure oxides [32]. It means the amount of the compositions is changed during sintering process because of many reason such as component vaporization. Moreover, there are other complexities such as different reactions including formation and decomposition of many phases, kinetic of ZnO grain growth, densification of melted additives during the ceramic fabrication. On other hand, the additives are not completely independent therefore; it is very difficult to consider the effect of one additive as a variable on the non-linearity as response while other additives are kept constant in the optimization process [33-34]. Whereas, the multivariate semi-empirical methods such as response surface methodology (RSM) and artificial neural network (ANN) have been widely accepted to model and optimize the productive processes [35-37]. The multivariate methods contemplate the effect of two initial ingredients (variables) on the final output product (response) simultaneously free of mentioned complexity [38]. In addition, the semi-empirical methods have used the responses of the designed actual experiments for modeling which are applied to optimize the process [36-41]. In this work, the fabrication of the ZnO-Bi_2O_3 based low voltage varistor were modeled and optimized by RSM and ANN. In the modeling, the amounts of the starting powders were selected as input variable while the non-linear coefficients of the fabricated varistors were the actual responses. The generated models of both RSM and ANN were validated by particular techniques then they were used to navigate the fabrication.

Experimental setup

Materials and methods

In this work, ZnO (99.9%), $Bi(NO_3)_3.5H_2O$ (98%, Alfa Aesar), $Ti(OC_4H_9)_4$ (96%, Alfa Aesar), Antimony acetate (99.99%, Aldrich), and absolute ethanol (Merck) were used to prepare starting powder. To prepare coated ZnO powder, the appropriate amount of $Bi(NO_3)_3.5H_2O$, Antimony acetate and $Ti(OC_4H_9)_4$ were dissolved in 100 ml of the ethanol under continuous stirring for 1 h. Then, the appropriate amount of ZnO powder was slowly added to the solution at 80 ^oC to obtain the slurry. The slurry was changed to paste with continual heating and magnetic stirring. The paste was dried by an oven at 100 ^oC overnight. Thereafter, the dried paste was ground and characterized by Field Emission Scanning Electron Microscopy (FESEM) and thermo-gravimetric analysis (TGA) to indicate coating layer and determine the calcinations temperature respectively. The FESEM confirmed the coated ZnO in this stage (Fig. 1). The calcinations was conducted at 750 ^oC for 2 h in air with a heating and cooling rate 5 ^oC/min to convert coated hydroxide ($Bi(OH)_2$, TiO_2 and $Sb(OH)_2$) to metal oxide (Bi_2O_3, TiO_2 and Sb_2O_3) by a box furnace (CMTS model HTS 1400). To make the varistor, the proper amount of coated ZnO powders as starting powder was pressed into 10 mm diameter pellets at 200MPa using a uniaxial presser machine. The compacted pellet was sintered at 1260 ^oC in air for 1 h, also with heating and cooling rates of 5 ^oC/min [38]. The both sides of sintered pellet as ceramic core of the varistor were painted by a silver electrode for DC current-voltage (I-V) characterization. The I-Vs were obtained by scanning the varistors from 0 to 100 volts using a step size of 2.5 which was performed by a Keithley 2400 sourcemeter. The obtained current density (J) and electrical

RSC Advances Accepted Manuscript

This journal is © The Royal Society of Chemistry [year]

field (E), the I and V were divided by surface of the painted silver electrode (cm^2) and thickness of the ceramic core (mm) respectively. The non-linear coefficient of the varistor which comes from $I = KV^{\alpha}$ (α = alpha) was calculated according to equation (1),

$$Alpha = \frac{LogJ_2 - LogJ_1}{LogE_2 - Log\,E_1} \qquad (1)$$

where E_1 (V/mm) and E_2 (v/mm) were obtained at J_1 = 0.1 (mA/cm^2) and J_2 = 1 (mA/cm^2), respectively [42]. The alpha was used to fitting and learning processes of used semi-empirical methods to obtain the optimized varistor. The optimized varistor was characterized by X-ray diffraction (XRD; (PANanalytica, Philips-X'pert Pro PW3040/60) and field emission scanning electron microscopy (FESEM; JEOL JSM-7200) with energy dispersive X-ray analysis (EDX). The XRD was within the 2θ scan range of 20-80°for the phase analysis.

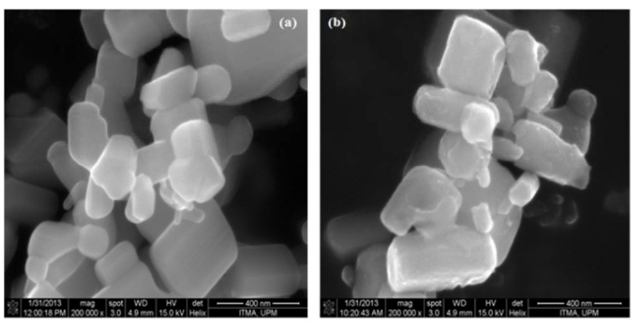

Fig. 1. The morphology of the used ZnO grain in the ceramic core of the low voltage varistor (a) ZnO powder before coating, (b) ZnO powder after coating and before calcination

RSM experimental design

RSM modeling as a semi-empirical method uses the actual responses which are obtained by particular experiment of design (EOD). In this case, the design was carried out by central composite design (CCD) that embedded in the Design-Expert software version 8.0.7.1, Stat-Ease Inc., USA [28-29]. In the design, the amounts of the additives (Bi_2O_3, TiO_2, and Sb_2O_3) in the ceramic starting powder were considered as the input effective variables. The amounts of the variables were selected to be in the vicinity of their reported range [16, 43-47]. Table 1 shows the variables in coded symbols as well as the actual values and ranges used in the design. Table 2 illustrates the design of 20 samples which categorized as follows: factorial points (8 samples), axial points (6 samples), and central points (6 samples). The central points are the replicated samples which were acquired to measure the experimental pure error. In the design, each raw shows the process of a varistor's fabrication (Run) which explained in section 2.1 while the columns indicate the amount of the additives, the calculated and model predicted alpha of the fabricated varistor. Therefore, the process in section 2.1 was carried out for each run in the laboratory. The calculated alphas presented in Table 2 (the actual responses) were used for the RSM fitting process to find the appropriate model which applied for optimization of the varistor (section 3.1) [48-49]. The fitting process proposed a provisional model which was deeply validated by analysis of variance (ANOVA). The model was used to track the optimum amount of the additives in the experimental design points as well as predict the desirable condition that maximizes the alpha of final varistor.

Table 1. The effective variable in the ceramics staring powder and their used levels for experiment of interest

Effective variables		Level of the variables					
Coded	Actual	The lowest (-α)	Low (-1)	Center (0)	High (+1)	The highest (+α)	Unit
x_1	Bi_2O_3	0.16	0.3	0.5	0.7	0.84	Mol%
x_2	TiO_2	0.16	0.3	0.5	0.7	0.84	Mol%
x_3	Sb_2O_3	0.13	0.2	0.3	0.4	0.47	Mol %

RSC Advances Accepted Manuscript

Table 2. Experimental design of the varistor's fabrication, the columns show the amounts of Bi_2O_3, TiO_2, Sb_2O_3, actual and model predicted alpha while the rows are varistors as samples

Run	Bi_2O_3 (mol %)	TiO_2 (mol %)	Sb_2O_3 (mol %)	Observed Alpha	Predicted Alpha
1	0.3	0.3	0.2	4.1	4.6
2	0.7	0.3	0.2	4.3	4.7
3	0.3	0.7	0.2	1.0	1.4
4	0.7	0.7	0.2	5.5	5.3
5	0.3	0.3	0.4	4.0	4.4
6	0.7	0.3	0.4	3.5	3.3
7	0.3	0.7	0.4	3.9	3.6
8	0.7	0.7	0.4	6.6	6.3
9	0.164	0.5	0.3	5.7	5.2
10	0.836	0.5	0.3	7.2	7.5
11	0.5	0.164	0.3	5.9	5.3
12	0.5	0.836	0.3	4.8	5.1
13	0.5	0.5	0.132	3.0	2.5
14	0.5	0.5	0.468	2.9	3.1
15	0.5	0.5	0.3	15.3	14.5
16	0.5	0.5	0.3	13.6	14.5
17	0.5	0.5	0.3	15.3	14.5
18	0.5	0.5	0.3	13.6	14.5
19	0.5	0.5	0.3	13.6	14.5
20	0.5	0.5	0.3	15.3	14.5

ANN learning

The learning process is carried out to determine the structure of ANNs semi-empirical model methods by using training and testing data sets. Therefore, the performed experiments in Table 2 were randomly split up into two sets as training and testing data sets using the option available in NeuralPower software version 2.5 [50-51]. The ANN structure consists of input, hidden and output layers while the input layer is made of initial variables (additives) and output layer has only one node as response (alpha). Since the learning process determines the number of the node in the hidden layer by using the splitted data sets. The number of nodes in the hidden layer was obtained by trial and error learning calculation which was examined from 1 to '15' nodes. The learning process was initially started with one node in the hidden layer to obtain a network (architecture) with 3 nodes input, 1 node in hidden and 1 node in output layer by a quick propagation algorithm (QP). The nodes in the input and output layers are kept constant during the process while number of the nodes in the hidden layers were varied up to 15. The examination of each node is repeated for10 times to avoid the random correlation due to the random initialization of the weights. Among the repeated examination, the architecture with the lowest Root mean squared error (RMSE) is selected for each node. Therefore, 15 architectures are obtained at the end of the learning process for QP algorithm. As a result of the learning process, the architecture with minimum RMSE is selected as a final topology for calculation of the coefficient of determination (R^2) and the percentage of absolute average deviation (AAD) (E.q. 2 and 3),

$$R^2 = 1 - \frac{\sum_{i=1}^{n} (y_i - y_{di})^2}{\sum_{i=1}^{n} (y_{di} - y_m)^2} \qquad (2)$$

$$AAD = \left\{ \left[\sum_{i=1}^{n} (|y_i - y_{di}| / y_{di}) \right] / n \right\} \qquad (3)$$

where 'n' is the number of points, 'y_i' is the predicted value, 'y_{di}' is the actual value, and 'y_m' is the average of the actual values. Therefore, the appropriate topologies were determined by minimum RMSE and ADD while the R^2 was at maximum value. The model was used to obtain the importance and optimum narrow level of the additives in the initial powder. In addition, the model predicted the optimum values of the additives to achieve the maximum alpha value.

The semi-empirical methods

A corner of RSM

RSM creates a functional relationship between variable-variable and variables-response(s) by using approximated low-degree polynomial models that consist of the variables and their coefficients. Equation 4 shows the second-order polynomial which RSM commonly uses for optimization process,

$$Y = \beta_0 + \sum_{i=1}^{n} \beta_i x_i + \sum_{i=1}^{n} \beta_{ii} x_i^2 + \sum_{i=1}^{n-1} \sum_{j=i+1}^{n} \beta_{ij} x_i x_j + \varepsilon \qquad (4)$$

where Y is the response of interest, β_0 is a constant term, β_i is the coefficient of the linear terms, β_{ii} demonstrates the quadratic term coefficient, and β_{ij} is the coefficient of the interaction terms. All of the coefficients are unknown. The x_i and x_j are control variables and "ε" is a random experimental error. The β's are estimated by a fitting process that uses the actual experimental responses. In the fitting process, the responses are fitted to the

This journal is © The Royal Society of Chemistry [year]
RSC Advances Accepted Manuscript

polynomial (Eq.(4)) by sequential model sums of squares (SMSS). SMSS compares the sufficiency of linear, two-factor interaction (2FI), quadratic, and cubic models using the statistical significance of adding new model terms, step-by-step in increasing order [52]. The comparison is presented by statistical evidence such as the F-value, predicted residual sum of squares (PRESS), adjusted R-squared (R_{Adj}), predicted R-squared (R_{pred}), and probability value (P-value). The PRESS is the sum of the squares of a model's prediction errors. The minimum value of the P-value and PRESS as well as the maximum value of R_{Adj}, R_{Pred}, and F-value are considered to determine the provisional model of the process [48, 53]. The provisional model is usually suggested by the software and is studied in detail using analysis of variance (ANOVA) [54]. The ANOVA indicates the significance of each term of the model, including the intercept, linear, interaction, and square terms. In fact, the adequacy of the model is certified by ANOVA and then the model is used to navigate the process. The model is able to track the optimum amount of the variables in the experimental design points by canonical and three-dimensional (3D) plots as the surface response. Moreover, the model is capable of predicting the desirable condition that maximizes the yield of the productive process.

ANN description

ANNs are semi-empirical modeling methods which use the actual processing condition and corresponding responses to govern a network to avoid of complexity. The network consists of different layers such as input, hidden and output which are made of several connected units (nodes). The nodes are simple artificial neurons which mimics a biological neural network make. The nodes of input layer are the effective variables and in output layer is the responses. In the hidden layer, the number of nodes is determined by learning process [55-56]. In the network, the nodes are connected by multilayer normal feed-forward or feed-back connection formula [57]. To qualify the network, the input layer acts as distributor and sends data via the weights to the nodes of second layer (hidden layer) [58]. The weighted data is saved as processing nodes in the hidden layer and then transferred to the output layer by particular transferred function [59-60]. Therefore, the qualified data are passed into the input layer, propagated to hidden layer and then transfers into the output layer of the network by iterative procedure [61]. The iteration is an act of repeating a process to approach a desire result. After appeared the first input-output iteration result, the second period is processed and so on. The network changes the weights in order to reduce the difference between actual and network's predicted responses at each iteration. The results of iteration are used as starting point of next iteration. For example, when the results of last iteration become almost equal to the results of previous iteration, the process will be terminated. The iteration process is continued by self-similarity method (Eq.5)[61].

$$S(B) = \sum_{I=1}^{m}[y_i - f(x_i\beta)^2] \quad (5)$$

where 'm' is an empirical data pairs of independent and dependent variables such as (x_i, x_i) and $f(x_i, \beta)$ is the model curve. In self-similarity process, the β parameter of $f(x_i, \beta)$ is optimized by minimizing the root mean squared error (RMSE). As a result, the main aim of the learning process is to find the weights for minimizing the RMSE which is obtained from difference between network prediction and actual responses (Eq. 6).

$$RMSE = (\frac{1}{n}\sum_{i=1}^{n}(y_i - y_{di})^2)^{\frac{1}{2}} \quad (6)$$

where 'n' is number of the points, y_i is the predicted values and y_{di} is the actual values.

Results and discussion

In this work the fabrication of ZnO-Bi_2O_3-TiO_2-Sb_2O_3 ceramic that is used as core of low voltage varistors was modeled and optimized to improve the protectiveness of electrical devices and consequently e-waste reduction. The modeling processes were carried out by semi-empirical methods such as RSM and ANN. In the processes the initial additives in the varistor's ceramic core starting powder including Bi_2O_3, TiO_2 and Sb_2O_3 were input variables while the non-linear property of the fabricated varistors (alpha) was output. The obtained models of the used methods were validated by different techniques then they were used to navigate the fabrication which included optimization of the input variables to maximize the output as well as determined the importance of the input variables. As final conclusion, the models predicted the optimum varistors which experimentally were fabricated. The electrical characteristic of the varistor were compared to select the final optimized varistor.

RSC Advances Accepted Manuscript

RSM modeling and validation

According to the experimental design (Table 2), twenty varistors were fabricated and their I-V characteristics were measured to calculate actual alpha which is presented by Fig. 1. As shown, the maximum alpha belonged to the middle of the selected levels of the additives that shows the levels were properly selected. To obtain a suitable model, the collected data in Table 2 as experimental design including the amount of the additives and observed alpha were used as input variables and output response for fitting process respectively by RSM. First, the fitting process were carried out for 2FI, linear, quadratic, and cubic models to obtain Lack of Fit indicators and the standard deviation (Std. Dev.), R_{Adj}, R_{Pred}, and R_{Pred} (Table 3). Then the results of each model were compared to suggest the provisional model for deeply validation (Table 4). As Table 4 indicates the quadratic model was merit to suggest while the cubic model was aliased. As a result, the quadratic model with Std. Dev. (0.8), R_{adj} (0.973), R_{pred} (0.951), and R^2 (0.986) was selected as the provisional model to deeply validation.

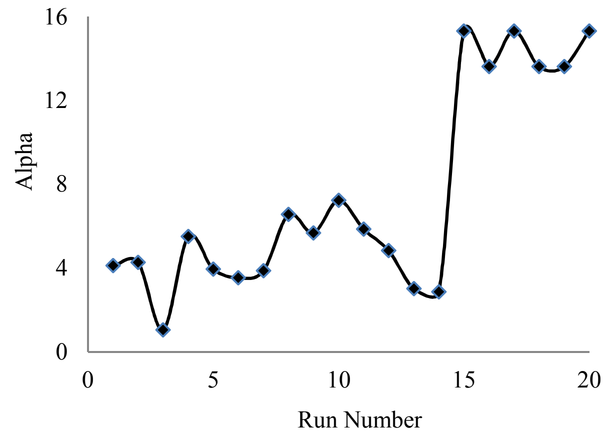

Fig. 2. The obtained actual alpha for 20 varistors in the experimental design while the run numbers 15 to 20 are replication which are in middle of the selected levels

Table 3. The fitting results of the 2FI, linear, quadratic and cubic models, Std.Dev. is standard deviation

Source	Lack of Fit indicator		Model Summary Statistics				
	F-Value	p-value	Std.Dev.	R_{Adj}	R_{Pred}	R^2	PRESS
Linear	46.9	0.0003	5.3	0.0	-0.2	-0.3	617.3
2FI	63.0	0.0001	5.8	0.0	-0.4	-1.5	1146.5
Quadratic	0.5	0.7789	0.8	1.0	1.0	1.0	22.5
Cubic	0.2	0.6830	0.9	1.0	1.0	0.9	42.2

Table 4. The sequential model sum of squares comparison for 2FI, linear, quadratic and cubic models to suggest the provisional

Source	F-Value	p-value	Remark
2FI vs. Linear	0.1	0.9578	
Quadratic vs. 2FI	225.8	< 0.0001	Suggested
Cubic vs. Quadratic	0.6	0.6519	Aliased

The selected provisional model which is a mathematic equation (E.q. 6) has presented the relationship between the inimical additives as input variables as well as the variables and final output (alpha) using estimated coefficients and linking signs (±).

$$Y = -55.244 + 68.436x_1 + 60.736x_2 + 242.182x_3 + 23.130x_1x_2 - 14.612x_1x_3 + 29.810x_2x_3 - 72.143x_1^2 - 81.49x_2^2 - 413.012x_3^2 \quad (6)$$

where Y is alpha; x_1, x_2, and x_3 are linear parameters, x_1^2, x_2^2, x_3^2 are the quadratic terms; and x_1x_2, x_1x_3, and x_2x_3 are the interaction factors which were introduced by Table 1. The next number to the items are fitting estimated coefficients which are the weights of the terms while the linked signs (+,-) determine the synergic and antagonistic behavior of the parameters in the model.

The deeply validation of the provisional model was carried out by analysis of variance (ANOVA) which has depicted in Table 5. As

This journal is © The Royal Society of Chemistry [year]

RSC Advances Accepted Manuscript

shown, the general model fit and lack of fit were correctly significant and not-significant respectively. As the detail of validation, the term's partial sum of squares has confirmed the significance of x_1, x_1x_2, x_1^2, x_2^2, and x_3^2 in the model while x_2, x_3, x_1x_3, and x_2x_3 were not significant, which means they can be removed from the model. Therefore, the modified model could be presented by:

$$Y = -55.244 + 68.436x_1 + 23.130x_1x_2 - 72.143x_1^2 - 81.49x_2^2 - 413.012x_3^2 \quad (7)$$

where the linear term of x_1 (Bi_2O_3) and the interaction term of x_1x_2 ($Bi_2O_3 \times TiO_2$) have a synergic effect on alpha, while the quadratic terms have an antagonistic effect on the response. Moreover, the importance of the terms is exhibited by the coefficients and their priority were appeared like $x_3^2 > x_2^2 > x_1^2 > x_1x_2 > x_1$. As result of the validation, the quadratic model has been recognized as outstanding final model which used to navigate the ceramic fabrication process.

Table 5. The model analysis of variance for model fit and lack of fit as well as the importance of the terms in the provisional model

Source	F-Value	p-value	Remark
Model Fit	78.27	< 0.0001	significant
Model Lack of Fit	0.48	0.7789	not significant
x_1	10.22	0.0095	significant
x_2	0.05	0.8335	not significant
x_3	0.82	0.3852	not significant
x_1x_2	10.62	0.0086	significant
x_1x_3	1.06	0.3275	not significant
x_2x_3	4.41	0.0621	not significant
x_{12}	185.58	< 0.0001	significant
x_{22}	239.73	< 0.0001	significant
x_{12}	380.48	< 0.0001	significant
Lack of Fit	0.48	0.7789	not significant

Model application

Levels optimization

The validated model optimized the input variables (Bi_2O_3, TiO_2, and Sb_2O_3) in range of the experimental design to obtain a varistor with maximum alpha. The optimization was carried out by mathematical derivation of the validated model (E.q (7)) and graphic three dimensional plots (3D plots) that produced the points and response surface for the additives as well as alpha respectively. The optimized points were obtained by equations (8) to (10) which only one parameter is varied [36-37].

$$\left[\partial Y / \partial x_1\right]_{x_1x_3} = 0 \quad (8)$$

$$\left[\partial Y / \partial x_2\right]_{x_1x_3} = 0 \quad (9)$$

$$\left[\partial Y / \partial x_3\right]_{x_1x_2} = 0 \quad (10)$$

where the variables x_1, x_2, and x_3 in the equations were introduced by Table 2. The calculation point method is very simple however its experimental validation test has presented a large error.

On the other hand, the response surface method has presented the effect of two variables (additives) on the output (alpha) in a 3D plot (Fig. 3) while the other parameter is kept constant. In this case, there are 3 variables such as TiO_2, Bi_2O_3, and Sb_2O_3 which indicated three 3D plots in Fig. 3(a), 3(b) and 3(c). Fig. 3(a) shows the simultaneous effect of TiO_2 and Bi_2O_3 on the alpha at constant amount of Sb_2O_3. As observed, the increasing amounts of TiO_2 and Bi_2O_3 up to 0.5 mol%, made the synergic effect on the alpha, while the amounts antagonistically operated to reduce the alpha beyond the optimum (0.5 mol%). Therefore, the optimum has been presented by a small surface as response instead of a point that reduced the error of the experimental validation of the varistor. Fig. 3(b) shows the interaction effect of Sb_2O_3 and Bi_2O_3 on the alpha at a constant amount of TiO_2 which depicted the alpha was increased up to 0.5 and 0.3 mol% of $Bi_2O_3$and Sb_2O_3, respectively. However, at the excess amounts of the additives, the alpha was decreased. Moreover, Fig. 3(c) demonstrates the effects of TiO_2 and Sb_2O_3 at a constant amount of Bi_2O_3. As shown in the both 3D plots, the maximum value of the alpha appeared at 0.3 mol% Sb_2O_3 and the amounts of Bi_2O_3 and TiO_2 were confirmed as indicated in Fig. 2(a). The amount of Sb_2O_3 was synergically affected from 0.2 to 0.3 mol% on the alpha and then it operated as antagonistic effect up to 0.4 mol%. The synergic effect of Sb_2O_3 may be due to densification of the ceramic matrix during the sintering process [62]. However, their antagonistic effect beyond optimum might be due to homogeneous segregation of the additives at this concentration [47, 63]. As a result, the optimum has determined the very narrow level

RSC Advances Accepted Manuscript

of Bi_2O_3, TiO_2 and Sb_2O_3 and quite small surface response around 14.52 for the alpha.

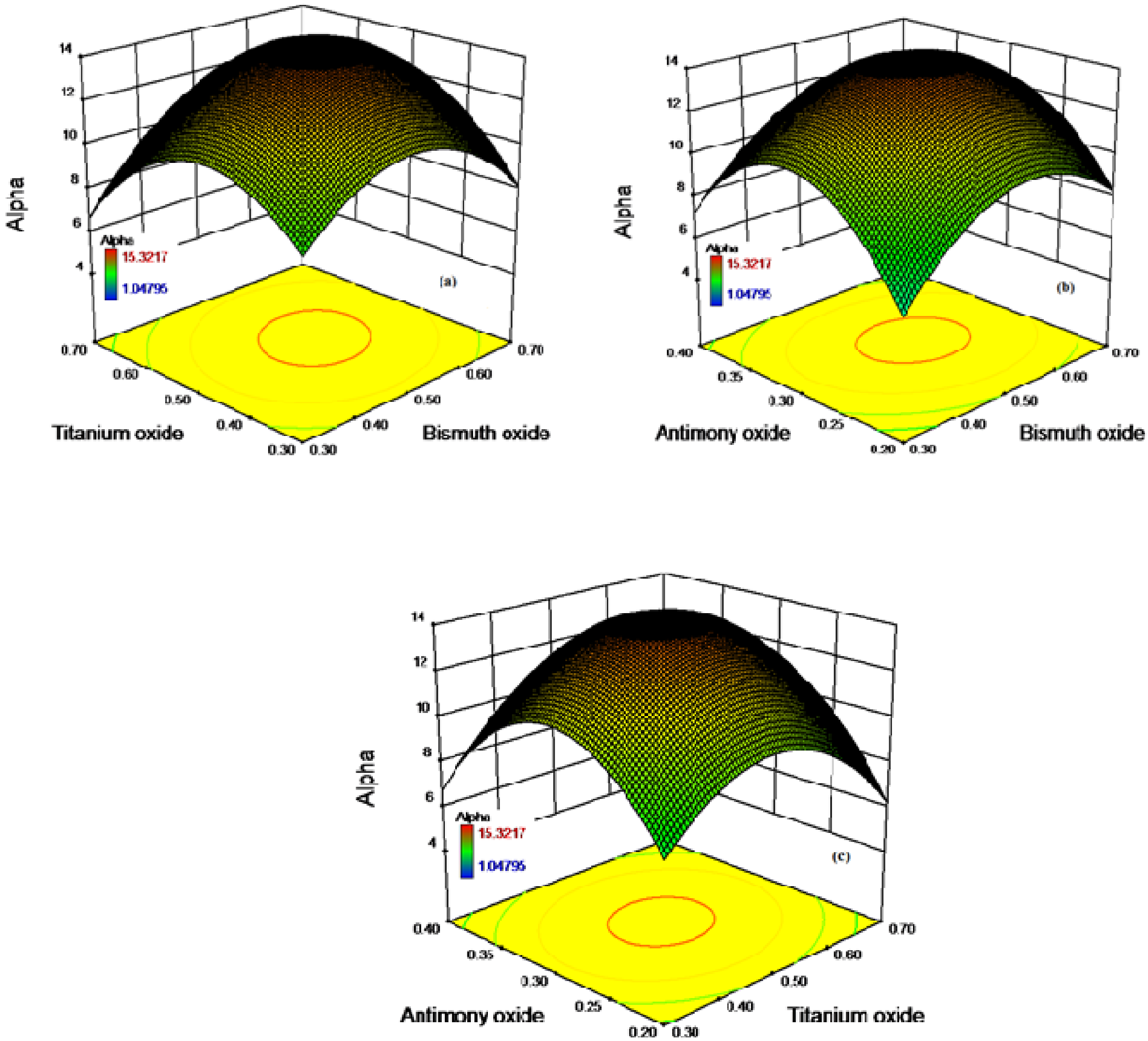

Fig.3. The graphical presentation of the maximized alpha response surface and optimized amounts of TiO_2, Bi_2O_3 and Sb_2O_3 as additive in the starting powder of the ceramic core that used in ZnO low voltage varistors, (a) The effect of TiO_2 and Bi_2O_3 on the alpha at constant amount of Sb_2O_3, (b) effect of Sb_2O_3 and Bi_2O_3 on the alpha at constant amount of TiO_2 (c) effect of TiO_2 and Sb_2O_3 on the alpha at constant amount of Bi_2O_3

The model prediction

The model was able to predict a varistor with maximum non-linearity coefficient (alpha) at high desirability value by using numerical particular condition which selected by experimenter. The desirability is an objective function that uses mathematical methods [64], where the range of the desirability starts from zero for out of the limited area and goes to one at the goal. The desirability of this prediction was 0.92 that was very close to the goal. The selected options of the particular condition were 'in range', 'minimum' and maximum for 'amount of the additives', 'standard error' and 'alpha' respectively. The options were facilitated by the default of used software. The model predicted values for Bi_2O_3, TiO_2 and Sb_2O_3 were 0.52, 0.5 and 0.3 mol% at

This journal is © The Royal Society of Chemistry [year]

RSC Advances Accepted Manuscript

standard error, 0.328, and alpha, 14.52. The suggested values of the additive were used to fabricate the ceramic core in the laboratory for further experimental validation. The both side of the ceramic were painted by silver electrode and used as final varistor to electrical characterization. Fig. 9 has been presented the results of the characterization which used to calculate the alpha at J_1 = 0.1 (mA/cm^2) and J_2 = 1 (mA/cm^2). The alpha was 15.3 for E_1= 7.4 (V/mm) and E_2 = 8.6 (V/mm).

ANN modeling and validation

The ANN modeling has determined the network structure of the ceramic fabrication by designation the hidden layer artificial node number. The node number was obtained by trial and error learning calculations which were examined from one to 20 nodes. The calculations were initially started with one node in the hidden layer to obtain the architecture with 3 input nodes, 1 node in hidden and 1 node in output layer by a QP algorithm. The nodes in the input and output layers were kept constant during the process while number of the nodes in the hidden layers were varied up to 20. The examination of each node is repeated for10 times to avoid the random correlation due to the random initialization of the weights. Among the repeated examination node number, the architecture with the lowest RMSE was selected to compare with other architectures. As Fig. 4 shows, the RMSE of 20 architectures were plotted versus their hidden layer node number at the end of the learning process. As a result of the learning process, the architecture with minimum RMSE is selected as a final topology which was validated by R^2 and AAD calculation.

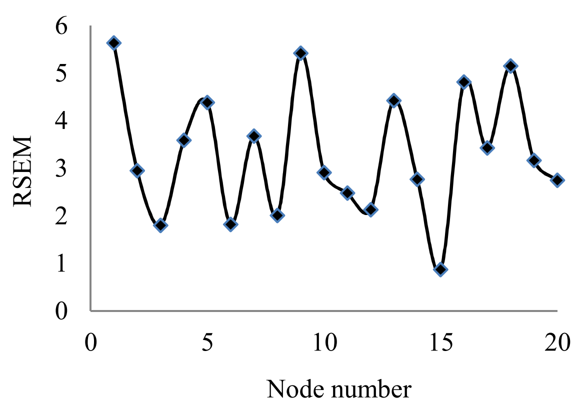

Fig.4. The RMSE of the learned hidden layer of the obtained topologies, the smallest RMSE belonged to the **topology that has 15** node in its hidden layer (QP-3-15-1)

The AAD calculation of the selected topology (QP-3-15-1) was 1.57 and 6.87 for training and testing data sets respectively which exhibited the reasonable minimum absolute average deviation. In addition, the scatter plots of actual alpha versus model predicted alpha of the varistors in the training and testing data sets to exhibit the R^2 of the QP-3-15-1 topologies (Fig. 5). As shown, the predicted values was so well fitted to the actual values for training data set (R^2 = 0.991) as well as testing date (0.974) sets which confirmed the validity of the topology (QP-3-15-1). Therefore, the QP-3-15-1 topology was considered as efficient final model for navigation of the ceramic fabrication (Fig. 6). In the model, the input variables such as Bi_2O_3, TiO_2 and Sb_2O_3 are connected to the calculated hidden nodes layer by multilayer normal feed-forward and then connect to alpha in output layer. The bias shifts the space of the nonlinearity properties. Therefore, the model has been applied to obtain the importance and optimized level of the additives in the starting power of the ceramic as well as predict the optimum values of the additives in the ceramic's starting powder to achieve the maximum non-linearity (alpha) for the varistor.

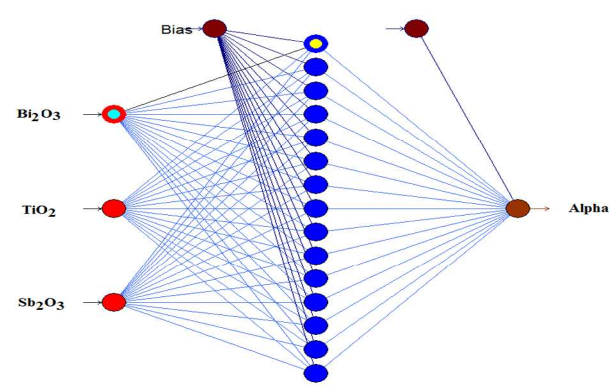

Fig. 6. The fabrication model structure of the ceramic core in ZnO based low voltage varistor, the model consists of 3 variables in input layer, 15 nodes in hidden layer and 1 response in output layer (QP-3-15-1), bias shifts the space of the non-linearity properties

RSC Advances Accepted Manuscript

Journal Name

RSC Advances

Dynamic Article Links ►

Cite this: DOI: 10.1039/c0xx00000x

www.rsc.org/xxxxxx

ARTICLE TYPE

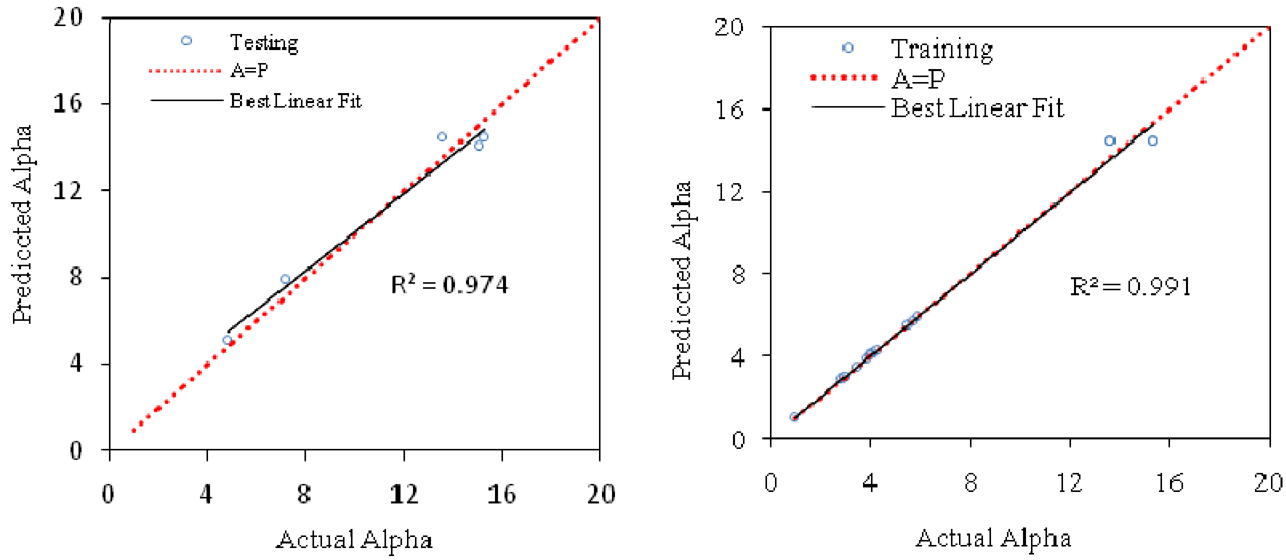

Fig. 5. The scatter plots of the actual and predicted alpha of the training and testing data set to visualize the R^2 of selected topology (QP-3-15-1)

Importance of the effective variables

Importance shows the relative effect (%) of the initial additives in starting powder of the ceramic core as input variables on the non-linearity of the varistor as response (Alpha). Therefore, the importance determines the effectiveness of the inputs as well as confirms or rejects the initial suppose for effective variables. In this case, the selected ANN model (Q-3-15-1) has determined the relative importance of Bi_2O_3, TiO_2 and Sb_2O_3 in starting power of the ceramic at optimum condition (Fig. 7). As shown, the relative importance was 9 % (Sb_2O_3), 33 % (TiO_2) and 22 % (Bi_2O_3). As a result, the selected additives variables were confirmed as effective input for the ceramic fabrication and none of them was neglect able in this work.

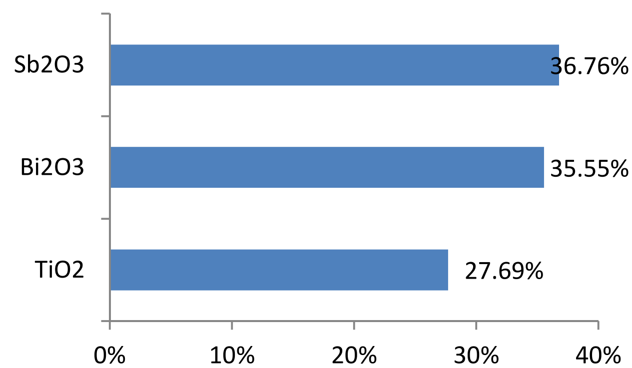

Fig. 7. The relative importance of Sb_2O_3 (36.76 %), Bi_2O_3 (35.55 %), and TiO_2 (27.69 %), as the used additives in starting powder of ceramic core for ZnO based low voltage varistor

Model applications

Level optimization

The wide levels of the additives in the starting power were selected according to previous works which were carried out by traditional methods such as one variable at a time [45]. Therefore, the levels were re-designed and optimized by the validated model (QP-3-15-1). For this purpose, the model simulated the effect of two additives on the alpha simultaneously without further requirement of mathematic function and equation knowledge while other factor was kept constant. The simulated effects have

RSC Advances Accepted Manuscript

been presented as three dimensional plots (3D plots) by Fig. 8 which demonstrate the surface of the additives' effect on the alpha. Therefore, the optimized narrow levels of the additives were Bi_2O_3 (0.606 – 0.836), TiO_2 (0.293 – 0.836) and Sb_2O_3 (0.154 – 0.301) in mol% at optimum condition. The levels were used to predict the optimum point value of the additives that maximized the alpha.

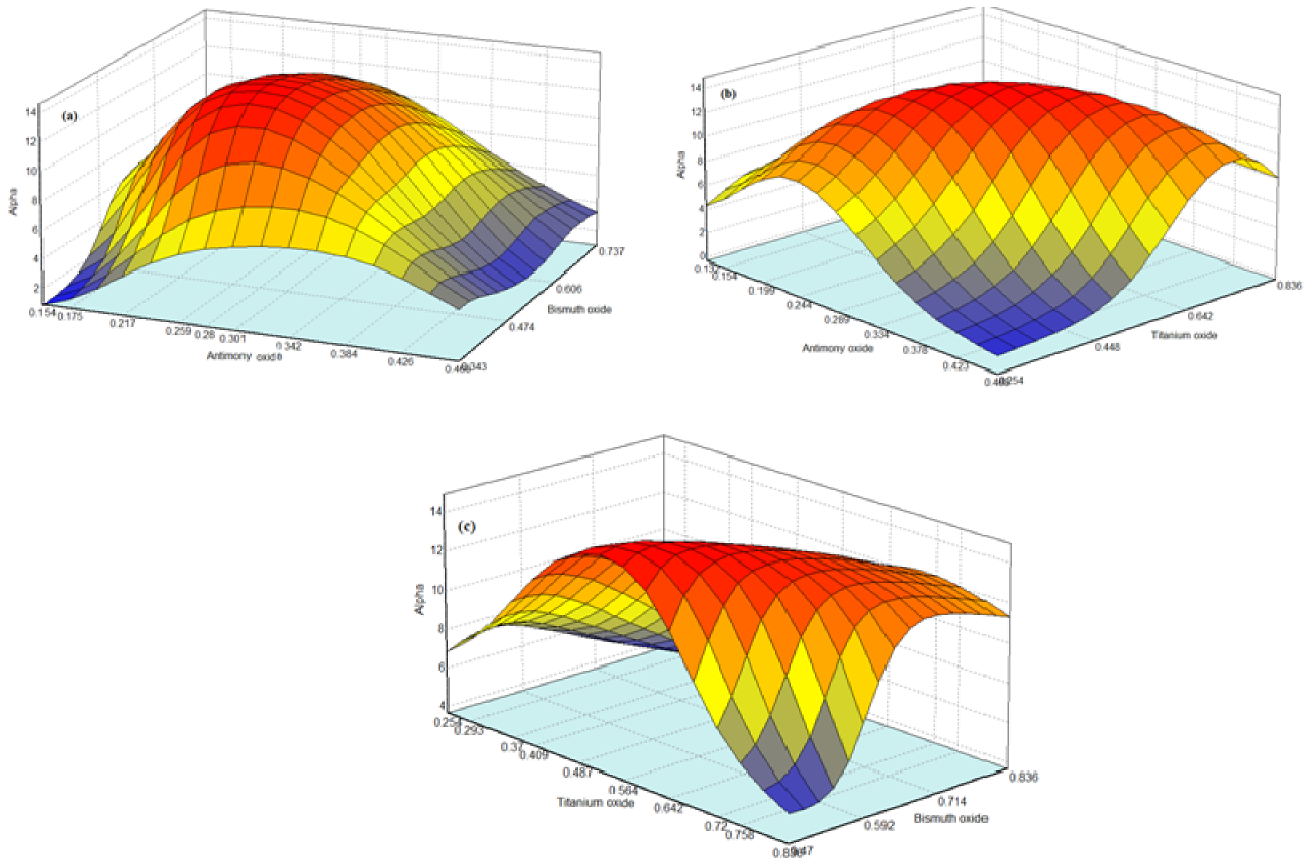

Fig. 8. The 3D plots of simultaneous effect of two additives on the alpha, the red surface response is the desirable alpha and blue color shows the lowest values of the alpha, (a) the effect of Sb_2O_3 and Bi_2O_3, (b) the effect of Sb_2O_3 and TiO_2 and (c) the effect of Bi_2O_3 and TiO_2

Model prediction

The model was used to predict the optimum condition in the optimized levels for fabrication of 3 varistors (Table 6). The table shows the optimum point values of the additives and the related alpha for each suggested varistors. The fabricated processes including preparation of the starting powder, pressing, sintering and electroding were carried out for the three varistors in the laboratory to validate the model prediction. The electrical characterization of the varistors was carried out to calculate the alpha (E.q 1) which indicated in table 6. As shown, the actual alphas were very close to the model prediction which confirmed the model predictability. Therefore, varistor 1 was selected as optimized case for electrical (E-J) and structural characterization including FESEM, EDX and XRD.

RSC Advances Accepted Manuscript

Table 6. The model predicted varistors that consists of the values of the additives in ceramics starting powder, the rows show the optimum amounts of the additives and the columns indicate the composition in the ceramic core of each varistors, the predicted alpha was suggested by model and the actual alpha is experimental result

Additives and alpha	Varistor 1	Varistor 2	Varistor 3
Bi_2O_3	0.50	0.4611	0.4611
TiO_2	0.47	0.468	0.437
Sb_2O_3	0.21	0.256	0.262
Predicted Alpha	27.24	27.21	26.90
Actual Alpha	28.10	27.74	26.44

The models navigation

In this work, the variables were initially used in wide levels, identical importance and without any considered points. Therefore, the RSM (E.q. 6) and ANN models (Fig. 6) were used to determine the optimum levels, optimum points and the importance of the effective variables which is presented by Table. 7. As shown, there is a big difference between the values of the obtained alpha from RSM and ANN predicted varistors which are 15.3 and 28.1 respectively. It might be due to the selected levels and consequently the used point values of the Sb_2O_3 in the ceramic starting powder. The Sb_2O_3 controls the growth of the ZnO grains which is necessary for low voltage varistors by decreasing the mobility of grain boundaries by making a fine Sb-rich film on the surface of the ZnO grains [65]. Moreover, the high models importance Sb_2O_3 confirmed that the alpha was very sensitive to the amount of while RSM's model (Eq. 6) has depicted the antagonistic effect of the additive on the alpha. As a final result of the modeling processes, ANN predicted varistor was selected to characterize the microstructure of the ceramic core by using XRD, FESEM and EDX.

Table 7. The results of application RSM and ANN validated models for additives of ceramic starting powder as input effective variables and non-linear properties of final optimized varistors

Model	Bi_2O_3			TiO_2			Sb_2O_3			Alpha
	Level (Mol%)	Point (Mol%)	Imp. (%)	Level (Mol%)	Point (Mol%)	Imp. (%)	Level (Mol%)	Point (Mol%)	Imp. (%)	
RSM	0.4 - 0.7	0.52	23	0.4 – 0.6	0.5	30	0.2 - 0.35	0.3	47	15.3
ANN	0.61 – 0.84	0.50	36.55	0.29 – 0.84	0.47	27.69	0.15 – 0.30	0.21	36.76	28.1

Starting powder of the final varistor

The starting powder of the final varistor ceramic core was prepared according to above methods (section 2.1). Fig. 9 shows the FESEM morphology of the starting powder which was calcined to produce the coated metal oxides over the ZnO grains. As Fig. 9 (a) indicated, the distribution of the coated additives has presented great homogeneity which confirmed the ability of the solution coating method for the fabrication. Moreover, the most frequent coated additives particles sizes were within 40 to 50 nm (Fig. 9b), as obtained from 100 particles in different images of the calcined powder.

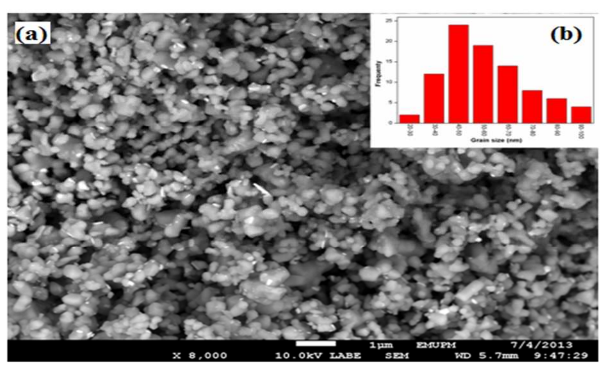

Fig. 9. The FESEM morphology of the calcined starting powder of the final varistor ceramic core, (a) the coated additives over ZnO grains, (b) the particles size of the coated additives

This journal is © The Royal Society of Chemistry [year]
RSC Advances Accepted Manuscript

Fig. 10. Illustrates the limited area EDX spectra of the starting powder to element analyze. As shown, the elements of Zn, Bi, Ti, and O were detected in the selected area of the powder while antimony (Sb) was not detected whereas it was detected by XRD (Fig not show).

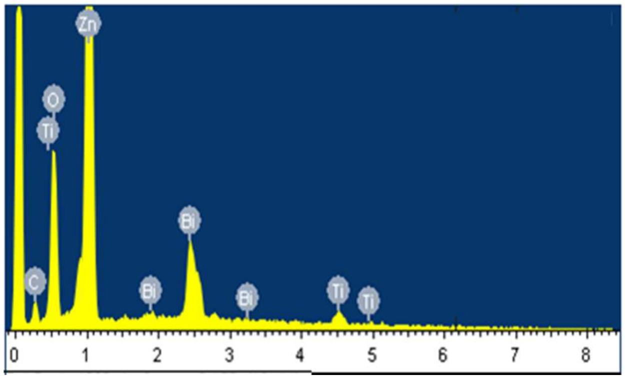

Fig. 10. The EDX histogram of the staring powder of final varistor ceramic core, the C peak is related to carbon type that used as based of the sample

The ceramic core of the final varistor

To prepare the ceramic core of the final varistor, the appropriate of staring powder was pressed into particular pellet then sintered at 1260^{o}C for one hour. The sintered pellet as ceramic core was characterized using FESEM, EDX, and XRD. Fig. 11 demonstrates the FESEM morphology of the ceramic core microstructure. Fig. 11(a) illustrates the homogenized ZnO grains size which may be due to the appropriate distribution of the additives in the initial powder [66]. The size frequency of the ZnO grains has presented by Fig. 11(b) which is in the range of 7 to 26 µm. As observed, the maximum frequency of the sizes was concentrated between 13 and14 µm that demonstrated the excellent enhancement of the grain size in the optimized comparison of the starting powder.

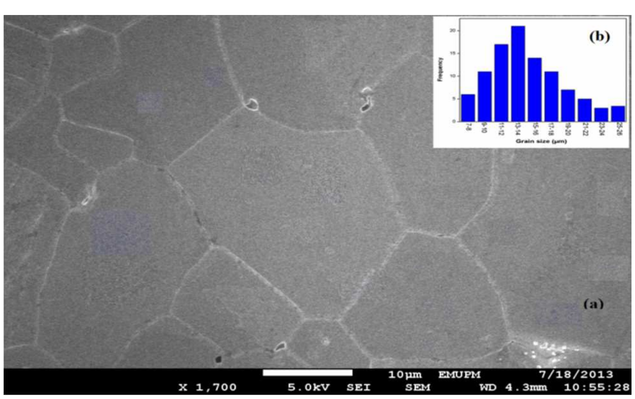

Fig. 11. The microstructure of the ceramic core in the low voltage varistor, (a) FESEM micrographs, (b) ZnO grains size distribution

The element analysis of the ceramic core has been investigated XRD pattern that reported according to the reference code such as 00-005-0664, 00-008-0258, 00-034-0097, and 00-025-1164 (Fig. 12). The XRD detected antimony element which has not detected by EDX analysis of the starting powder.

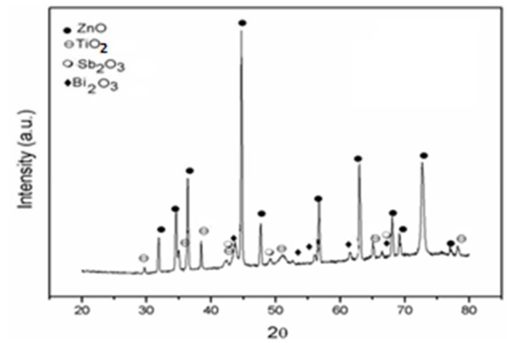

Fig.12. The XRD pattern of the ceramic core used in the optimized varistor

Conclusions

In this work, the fabrication of the used ceramic in voltage dependent varistor was designed and then experimentally performed to calculate its non-linear coefficients as output actual responses. The responses were used to obtain the appropriate model for the fabrication by RSM and ANN semi-empirical methods. The obtained models were carefully validated by mathematical, statistical and experimental evidences. Then the models were used to determine the importance of the effective additives, confirmed the selected levels of the initial additives in experimental design and the optimum points of the additives which were able to maximize the quality of the varistors. Thereafter, the collected results of the two models were compared to select the final varistor. As a result of the comparison, the highest quality protection, 28.1, was provided by the varistor which made of Bi_2O_3 (0.5 mol %), TiO_2 (0.47 mol %) and Sb_2O_3 (0.21 mol %). Therefore, the modeling and optimization successfully predicted the quit high protective varistor free of mathematical and physical complexity which has industrial scale up potential to produce high protected electronics which control the global e-waste.

RSC Advances Accepted Manuscript

Acknowledgments

The author would like to express acknowledgment to University of Malaya for granting this project under Research Grant, No: RP006F-13SUS and PR007D-13AET.

Notes and references

[a]Department of Electrical Engineering, Faculty of Engineering, University of Malaya, 50603 Kuala Lumpur, Malaysia
[b]Material Synthesis and Characterization Laboratory, Institute of Advanced Technology, Universiti Putra Malaysia, 43400, Serdang, Selangor, Malaysia
[c]Department of Mechanical Engineering, Faculty of Engineering, 50603 Kuala Lumpur, Malaysia
[d]Department of Chemistry, Faculty of Science, University of Malaya, 50603 Kuala Lumpur, Malaysia
[e]Institute of Hydrogen Economy, Energy Research Alliance, International Campus, Universiti Teknologi Malaysia, 54100 Kuala Lumpur, Malaysia
*corresponding author: Email: yadollahabdollahi@yahoo.com

1. Wath, S.B., P. Dutt, and T. Chakrabarti, Environmental monitoring and assessment, 2011. 172, 249-262.
2. Robinson, B.H., Science of the Total Environment, 2009. 408, 183-191.
3. Standler, R.B. 2012: Courier Dover Publications.
4. Avery, L.R., in *Secondary*. 1983, Google Patents.
5. Einzinger, R., Applications of Surface Science, 1978. 1, 329-340.
6. Nahm, C.-W., Materials science in semiconductor processing, 2013. 16, 1308-1315.
7. Bowen, L.J. and F.J. Avella, Journal of Applied Physics, 1983. 54, 2764-2772.
8. Brown, K., IAEI News March, 2004.
9. Greuter, F. and G. Blatter, Semiconductor Science and Technology, 1999. 5, 111.
10. Olsson, E., L. Falk, G. Dunlop, and R. Österlund, Journal of Materials Science, 1985. 20, 4091-4098.
11. Toplan, H.Ö. and Y. Karakaş, Ceramics international, 2001. 27, 761-765.
12. Clarke, D.R., Journal of the American Ceramic Society, 1999. 82, 485-502.
13. Gupta, T.K., Journal of materials research, 1992. 7, 3280-3295.
14. Wong, J., Journal of Applied Physics, 1980. 51, 4453-4459.
15. Pan, W.H., S.T. Kuo, W.H. Tuan, and H.R. Chen, International Journal of Applied Ceramic Technology, 2010. 7, E80-E88.
16. Zhang, C., D. Zhou, W. Lu, and Y. Hu, Journal of Materials Science: Materials in Electronics, 2001. 12, 357-360.
17. Ezhilvalavan, S. and T. Kutty, Materials Chemistry and Physics, 1997. 49, 258-269.
18. Mantas, P. and J. Baptista, Journal of the European Ceramic Society, 1995. 15, 605-615.
19. Eda, K., Journal of Applied Physics, 1978. 49, 2964-2972.
20. Gupta, T.K., Journal of the American Ceramic Society, 1990. 73, 1817-1840.
21. Blatter, G. and F. Greuter, Physical Review B, 1986. 33, 3952.
22. Sedky, A., T. Ali, and S. Mohamed, Journal of Physics and Chemistry of Solids, 2011.
23. Banerjee, A., T. Ramamohan, and M. Patni, Materials Research Bulletin, 2001. 36, 1259-1267.
24. Wang, M.-h., C. Yao, and N.-f. Zhang, Journal of Materials Processing Technology, 2008. 202, 406-411.
25. Inada, M., Japanese Journal of Applied Physics, 1980. 19, 409.
26. Olsson, E., G. Dunlop, and R. Österlund, Journal of the American Ceramic Society, 1993. 76, 65-71.
27. Metz, R., H. Delalu, J. Vignalou, N. Achard, and M. Elkhatib, Materials Chemistry and Physics, 2000. 63, 157-162.
28. Ezhilvalavan, S., Kutty, TRN, Materials chemistry and physics, 1997. 49, 258-269.
29. Levinson, L. and H. Philipp, Am. Ceram. Soc. Bull. Am. Ceram. Soc. Bull., 1986. 65, 639.
30. Zhang, C., Y. Hu, W. Lu, M. Cao, and D. Zhou, Journal of the European Ceramic Society, 2002. 22, 61-65.
31. Feng, H., Z. Peng, X. Fu, Z. Fu, C. Wang, L. Qi, and H. Miao, Journal of Alloys and Compounds, 2010. 497, 304-307.
32. Peiteado, M., M. De la Rubia, M. Velasco, F. Valle, and A. Caballero, Journal of the European Ceramic Society, 2005. 25, 1675-1680.
33. Wong, J., Journal of Applied Physics, 1980. 51, 4453-4459.
34. Senda, T. and R.C. Bradt, Journal of the American Ceramic Society, 1990. 73, 106-114.
35. Montgomery, D.C. 2008, New York: John Wiley & Sons Inc.
36. Abdollahi, Y., Zakaria, Azmi, Abdullah, Abdul Halim, Masoumi, Hamid Reza Fard, Jahangirian, Hossein, Shameli, Kamyar, Rezayi, Majid, Banerjee, Santo, Abdollahi, Tahereh, Chemistry Central Journal, 2012. 6, 1-8.
37. Abdollahi, Y., Zakaria, Azmi, Matori, Khamirul Amin, Shameli, Kamyar, Jahangirian, Hossein, Rezayi, Majid, Abdollahi, Tahereh, Chem Cent J, 2012. 6, 1-5.
38. Abdollahi, Y., A. Zakaria, R. Aziz, S. Tamili, K.A. Matori, N. Shahrani, N.M. Sidek, M. Dorraj, and S. Moosavi, Chemistry Central Journal, 2013. 7, 137-143.
39. Abdollahi, Y., Zakaria, Azmi, Abbasiyannejad, Mina, Masoumi, Hamid Reza Fard, Moghaddam, Mansour Ghaffari, Matori, Khamirul Amin, Jahangirian, Hossein, Keshavarzi, Ashkan, Chemistry Central Journal, 2013. 7, 1-7.
40. Abdollahi, Y., N.A. Sairi, M.K. Aroua, H.R.F. Masoumi, H. Jahangirian, and Y. Alias, Journal of Industrial and Engineering Chemistry, 2014.
41. Abdollahi, Y., A. Zakaria, N.A. Sairi, K. Amin Matori, H.R. Fard Masoumi, A.R. Sadrolhosseini, and H. Jahangirian, The Scientific World Journal, 2014. 2014.
42. Bernik, S., P. ZupanÄ iÄ , and D. Kolar, Journal of the European Ceramic Society, 1999. 19, 709-713.
43. Makovec, D., D. Kolar, and M. Trontelj, Materials research bulletin, 1993. 28, 803-811.
44. Li, Y., G. Li, and Q. Yin, Materials Science and Engineering: B, 2006. 130, 264-268.
45. Wang, Q., Y. Qin, G. Xu, L. Chen, Y. Li, L. Duan, Z. Li, Y. Li, and P. Cui, Ceramics International, 2008. 34, 1697-1701.
46. Xu, D., X.-n. Cheng, X.-h. Yan, H.-x. Xu, and L.-y. Shi, Transactions of Nonferrous Metals Society of China, 2009. 19, 1526-1532.
47. Cheng, L., G. Li, K. Yuan, L. Meng, and L. Zheng, Journal of the American Ceramic Society, 2012. 95, 1004-1010.

RSC Advances Accepted Manuscript

 This journal is © The Royal Society of Chemistry [year]

48. Anderson, M.J. and P.J. Whitcomb. 2005, Virginia: Productivity Pr.
49. Oehlert, G.W. Vol. 1. 2000: WH Freeman New York.
50. Sanchooli, M. and M. Ghaffari Moghaddam, Journal of chemical engineering of Japan, 2012. 45, 373-379.
51. Moghaddam, M.G. and M. Khajeh, Food and Nutrition, 2011. 2, 803-808.
52. Deming, S., Chemtech, 1989. 19, 249-255.
53. P. J. Whitcomb and M. J. Anderson. 2004, New York: Productivity Press.
54. Sen, R. and T. Swaminathan, Biochemical Engineering Journal, 2004. 21, 141-148.
55. Despagne, F. and D.L. Massart, Analyst, 1998. 123, 157-178.
56. Pareek, V., M. Brungs, A. Adesina, and R. Sharma, Journal of Photochemistry and photobiology A: Chemistry, 2002. 149, 139-146.
57. Ghaffari, A., H. Abdollahi, M. Khoshayand, I.S. Bozchalooi, A. Dadgar, and M. Rafiee-Tehrani, International Journal of Pharmaceutics, 2006. 327, 126-138.
58. Baş, D. and İ.H. Boyacı, Journal of Food Engineering, 2007. 78, 846-854.
59. Jorjani, E., S. Chehreh Chelgani, and S. Mesroghli, Fuel, 2008. 87, 2727-2734.
60. Göb, S., E. Oliveros, S.H. Bossmann, A.M. Braun, R. Guardani, and C.A. Nascimento, Chemical Engineering and Processing: Process Intensification, 1999. 38, 373-382.
61. Mandelbrot, B.B., Science, 1967. 156, 636-638.
62. Souza, F., J. Gomes, P. Bueno, M. Cassia-Santos, A. Araujo, E. Leite, E. Longo, and J. Varela, Materials chemistry and physics, 2003. 80, 512-516.
63. Lao, Y.-W., S.-T. Kuo, and W.-H. Tuan, Journal of Electroceramics, 2007. 19, 187-194.
64. Myers, R.H. and C.M. Anderson-Cook. Vol. 705. 2009: Wiley. com.
65. Bernik, S., N. Daneu, and A. Rečnik, Journal of the European Ceramic Society, 2004. 24, 3703-3708.
66. Shi, J., Q. Cao, Y. Wei, and Y. Huang, Materials Science and Engineering: B, 2003. 99, 344-347.

RSC Advances Accepted Manuscript

This journal is © The Royal Society of Chemistry [year]